Nanoscale

View Online
Dynamic Article Links

Cite this: DOI: 10.1039/c1nr10266d

www.rsc.org/nanoscale

PAPER

Highly active and enhanced photocatalytic silicon nanowire arrays†

Feng-Yun Wang,[a] Qing-Dan Yang,[a] Gang Xu,[a] Ngai-Yu Lei,[a] Y. K. Tsang,[a] Ning-Bew Wong*[a] and Johnny C. Ho[b]

Received 11th March 2011, Accepted 19th May 2011
DOI: 10.1039/c1nr10266d

Nanoporous and nonporous three-dimensional silicon nanowire arrays (SiNWAs) prepared with metal-assisted chemical etching method were investigated as photocatalysts in dye photodegradation systematically. In comparison with nonporous SiNWAs, nanoporous SiNWAs have higher surface area, larger pore volume, stronger light absorption and better photocatalytic activity. After the HF-treatment, the photocatalytic activity of all kinds of SiNWAs increased significantly and the nanoporous SiNWAs showed excellent stability. The photocatalytic activity of different types of SiNWAs with hydrogen surface termination can be recovered by HF treatment. This study also reveal that the hydrogen terminated surfaces on silicon nanowires (SiNWs) enhance the performance of SiNWAs by increasing their photocatalytic activity.

Introduction

Visible-light photocatalysis has attracted much interest because of its potential in utilizing solar energy to degrade organic pollutants.[1–7] In practical applications, it is important to select an economic route to design novel nanomaterials with good catalytic activity and high recovery.[8] A promising strategy is to load the catalyst on a substrate so that the catalyst can be easily recycled and reused.[9–11] Nowdays, TiO_2 is one of the most extensively studied semiconductor photocatalysts, which has an outstanding stability against corrosion.[12–15] However, its large bandgap (3.2 eV) significantly limits its applications in visible-light photocatalysis.[16,17]

Recently, studies of elemental semiconductors, such as silicon (Si), utilizing their applications in electronics, biological probes and energy,[18–22] have reported their promising photocatalytic activity in visible light.[23–27] Shao *et al.* showed the first example of SiNWs synthesized by oxide-assisted growth method for photocatalytic degradation of dye and photocatalytic oxidization of benzyl alcohol.[26] His work also exhibited superior photocatalytic activity of HF-treated SiNWs over most of the noble metal-modified SiNWs. Independently, Megouda *et al.* investigated the performance of hydrogen-terminated SiNWs and two kinds of metals decorated SiNWs for the degradation of dye molecules. The results indicated that hydrogen-terminated SiNWs exhibited better photocatalytic activity than the Ag and Cu modified SiNWs, except when the density of Cu nanoparticles on the SiNWs was significantly large.[27] These imply that the HF treatment is a convenient and an efficient way for improving the photocatalytic efficiency of SiNWs. Duan and his co-workers fabricated the nanoporous SiNWs from the n-type Si wafer with the resistivity of 0.008–0.02 Ω cm by the metal-assisted chemical etching approach. The porous SiNWs had large surface area up to 337 $m^2\ g^{-1}$ and displayed good photocatalytic activity after Pt modification.[28,29] Moreover, even though the p-type porous SiNWs has been reported previously,[30] the photocatalytic experiment has not been performed yet.

Much effort has been made to fabricate SiNWs by top-down methods such as chemical etching[31–35] and reactive ion etching,[36] and bottom-up methods such as laser ablation,[37,38] thermal evaporation decomposition[39] and chemical vapor deposition.[40] In this work, two kinds of porous and two kinds of nonporous SiNWAs have been synthesized by a rapid and facile two-steps metal-assisted chemical etching method from commercial single crystal Si wafers, which ensure the recovery and efficient reuse of catalyst (SiNWs).[35] Photocatalytic activity and recyclability of the SiNWAs before and after HF-treatment as photocatalysts on organic environmental contaminants was investigated.

Experiments

Synthesis of SiNWAs

Four samples of SiNWs arrays were prepared by the metal-assisted chemical etching method from two different n-type Si (100) wafers with the resistivity of 0.005–0.02 Ω cm, 1–10 Ω cm, respectively and another two different p-type Si (100) wafers with the resistivity of 0.001–0.005 Ω cm, 7–13 Ω cm,

[a]*Department of Biology and Chemistry and Center of Super-Diamond and Advanced Films (COSDAF), City University of Hong Kong, Kowloon, Hong Kong, 999077, China. E-mail: bhnbwong@cityu.edu.hk; Fax: +852-3442-7406; Tel: +852-3442-7817*

[b]*Department of Physics and Materials Science, City University of Hong Kong, Hong Kong, 999077, China*

† Electronic Supplementary Information (ESI) available: the optical spectrum of the 150 W halogen lamp used in the photocatalytic reaction; the photograph of the large-area samples of SiNWAs and polished p-type heavily doped Si wafer. See DOI: 10.1039/c1nr10266d

respectively.[35] The wafers were cut into 0.9 × 0.9, 1.8 × 1.8 and 3.6 × 3.6 cm^2 squares, washed with DI water, ethanol, acetone under sonication and immersed into the oxidant solution containing H_2SO_4 (97%) and H_2O_2 (35%) in a volume ratio of 3 : 1 for 30 min under room temperature to remove organic contaminants and to form a thin oxide layer. The cleaned wafers were etched with 5% HF aqueous solution for 3 min to form H-terminated Si surfaces and then immediately placed into a solution of 0.005 M $AgNO_3$ and 4.8 M HF for 1 min under ambient atmosphere. After a uniform layer of Ag nanoparticles (AgNPs) being coated, the wafers were washed with DI water to remove the excess Ag^+ ions and then immersed in the etchant composed of 4.8 M HF and 0.4 M H_2O_2. Different etching times were applied to make similar lengths for n-type heavily doped SiNWs (60 min), n-type lightly doped SiNWs (50 min), p-type heavily doped SiNWs (90 min) and p-type lightly doped SiNWs (75 min). After etching in dark at room temperature, silver particles were removed from the nanowires by immersing the wafers in aqueous HNO_3 solution with volume ratio of 1 : 1 for 1 h. The resultant samples etched from n-type heavily and lightly doped Si wafers, p-type heavily and lightly doped Si wafers were named as n-^{p}SiNWAs, n-SiNWAs, p-^{p}SiNWAs and p-SiNWAs, respectively.

HF-treatment for as-synthesized SiNWAs

In order to compare the photocatalytic properties of SiNWs before and after the HF treatment, the as-synthesized SiNWAs were treated with dilute aqueous HF solution again, producing hydrogen-terminated SiNWAs. Correspondingly, the hydrogen-terminated samples of n-^{p}SiNWAs, n-SiNWAs, p-^{p}SiNWAs and p-SiNWAs are shorted for H-n-^{p}SiNWAs, H-n-SiNWAs, H-p-^{p}SiNWAs and H-p-SiNWAs, respectively.

Characterization of the porous and nonporous SiNWAs

The morphologies of porous and nonporous samples were characterized with scanning electronic microscopy (SEM) (Philips XL30 FEG, with an accelerating voltage of 10 kV). The SiNWs were first scraped from the substrates and dispersed in ethanol by sonication for 10 min, and then deposited on a carbon-coated copper grid, which was used as a transmission electronic microscopy (TEM) specimen. The microstructure of the as-synthesized and HF-treated SiNWs were studied by TEM (Philips Technai 12 under 80 kV operation voltage), and the growth direction and crystalline quality of HF-treated SiNWs were investigated by HRTEM (Philips CM200, operating under 200 kV). Nitrogen adsorption and desorption isotherms were measured using a Quantachrome NOVA 1200e sorption analyzer at 77 K. Before measurements, the samples were also removed from the intact wafers by scraping with a razor blade and then degassed at 250 °C overnight in vacuum. The specific surface areas (S_{BET}) were measured by the Brunauer–Emmett–Teller (BET) method, where the pore size distributions were calculated from the adsorption branches of isotherms using BJH (Barett–Joyner–Halenda) model and the total pore volumes (V_{total}) were estimated from the adsorbed amount at a relative pressure P/P_0 of 0.99. The absorption spectra of the samples were conducted on LAMBDA 750 UV–Vis spectrophotometer.

Photocatalytic ability of porous and nonporous SiNWAs

Photodegradation experiments were carried out in a 50 mL conical flask containing 30 ml methyl red (MR) solution with initial concentration of 1 × 10^{-4} M under stirring. The reaction system was illuminated under a 150 W halogen lamp (light intensity of 135 mW cm^{-2}) with the optical range of 400–800 nm and the optical spectrum is shown in Fig. S1. The concentration of MR was determined using HP Agilent 8453 ultraviolet-visible (UV–Vis) spectrophotometer by monitoring the absorption peak at λ_{max} = 515 nm. The MR solution and intermediates of the reactions were analyzed through the Applied Biosystems 3200.

Q Trap tandem mass spectrometer, equipped with an electrospray source and operated in the positive ion mode.

Results and discussion

Characterization of SiNWAs

In order to study the morphology and structure of the SiNWAs and individual SiNWs, SEM and TEM measurements were performed. The SEM images of as-synthesized SiNWAs are displayed in Fig. 1a, 1b, 1c and 1d showing the large-scale top view images with 45° tilt for SiNWAs etched from n-type heavily and lightly doped, p-type heavily and lightly doped Si wafers, respectively, where the insets are selected images in high magnification. From top view images, all four samples have

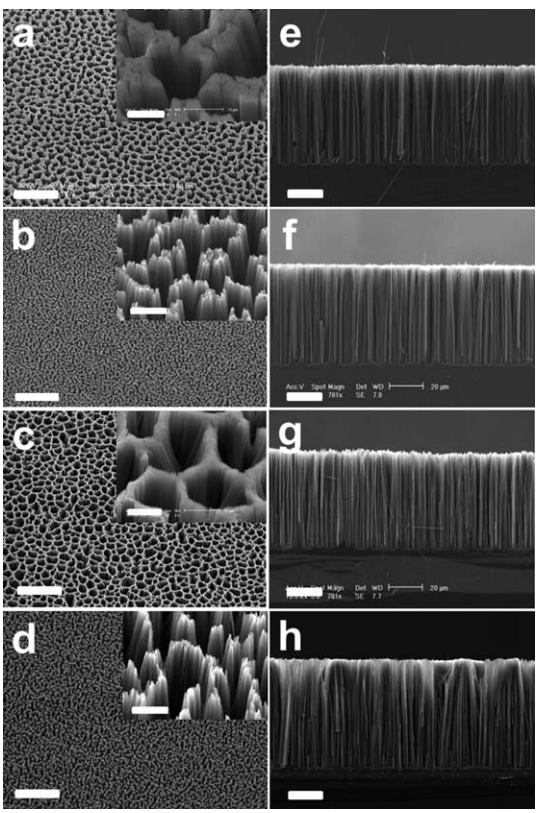

Fig. 1 SEM images of n-^{p}SiNWAs (a and e), n-SiNWAs (b and f), p-^{p}SiNWAs (c and g), and p-SiNWAs (d and h). Insets are the corresponding magnified top view images. The scale bars for top view images (a-d), cross section images (e-h) and insets are 100, 20 and 10 μm, respectively.

uniform surface and some congregated bundles of SiNWs which may be caused by the electrostatic attraction among them. The photograph of the large-area samples shown in Fig. S2 also indicates the uniformity of the four kinds of SiNWAs.† Whereas, the morphologies of SiNWAs etched from the heavily doped Si wafers are obviously different from those fabricated from the lightly doped Si wafers. By comparing Fig. 1a, 1b, 1c, and 1d and their corresponding insets, the density of SiNWs on the heavily doped Si wafer is less than that on the lightly doped one of the same type and the least was found on the p-type heavily doped Si wafer, which was indicated by the SiNWs coverage on silicon wafer surface. Fig. 1e, 1f, 1g and 1h are the magnified cross-section view of the corresponding left SiNWAs, where all kinds of SiNWs are similar. The wires with approximate 60 μm in length are distinguishable, uniform, straight and vertical to the substrate surface. According to the cross-section SEM images, the densities of the four different kinds of SiNWs are in roughly the same oder of magnitute, 10^{10} cm^{-2}, and the density of the SiNWs on the heavily doped Si wafers is even lower. However, the representative TEM images display obviously different structures between heavily and lightly doped SiNWAs: to the heavily doped SiNWAs (Fig. 2a and 2c), there are many pores in the bodies of wires shown as light spots and the pore sizes are similar in the two kinds of SiNWs ranging from 3 to 13 nm; to the lightly doped SiNWAs (Fig. 2b and 2d), in contrast, there is almost no pore on the wires observed. According to the numerous TEM images, the diameters of wires for all samples can be assessed in a range of approximately from 60 to 200 nm.

The SEM images of SiNWAs after HF-treatment are shown in Fig. 3. Compared with the as-synthesized ones, the four kinds of SiNWAs after HF-treatment are still uniform, straight and vertical to the substrate surface, and there is also no significant change on their lengths. The SiNWs are conglomerated at the tips, while the bundles are somewhat loose, which may be caused by the repulsive force formed in the surface of H-SiNWs.

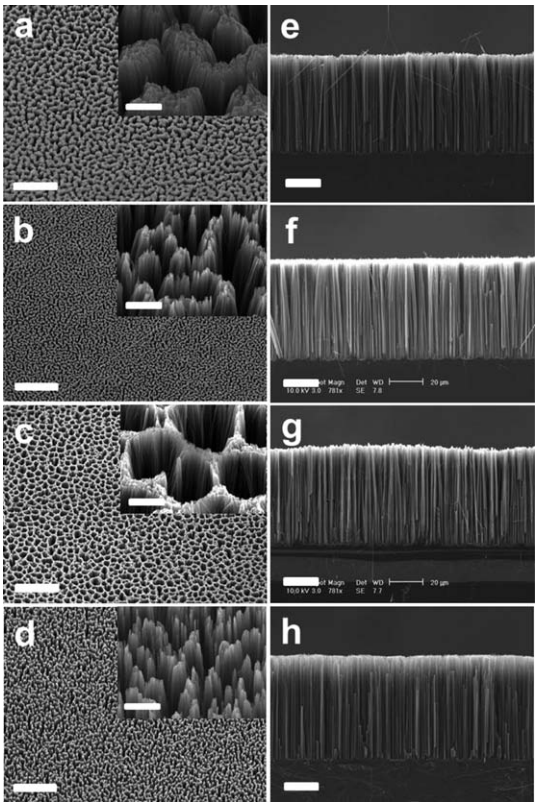

Fig. 3 SEM images of H-n-^{P}SiNWAs (a and e), H-n-SiNWAs (b and f), H-p-^{P}SiNWAs (c and g), and H-p-SiNWAs (d and h). Insets are the relative magnified top view images. The scale bars for top view images (a-d), cross section images (e-h) and insets are 100, 20 and 10 μm, respectively.

Notably, TEM images show that the pores are clearer than that of the as-synthesized samples due to the removal of amorphous silicon oxide layers (Fig. 3e and 3g). As shown in Fig. 3f and 3h, the difference of lightly doped SiNWs before and after HF treatment is insignificant. Therefore, the morphologies of four kinds of SiNWs remained almost unchanged after the HF-treatment. HRTEM images reveal that there are phase contrast caused by the nanopores on the edge and in the interiors of H-n-^{P}SiNW (Fig. 4a and 4e) and H-p-^{P}SiNW (Fig. 4c and 4g), which was not observed in the nonporous H-n-SiNWs (Fig. 4b

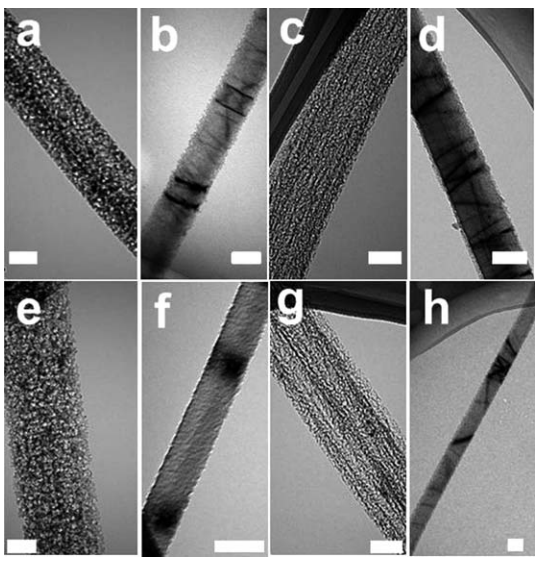

Fig. 2 TEM images of n-^{P}SiNW (a), n-SiNW (b), p-^{P}SiNW (c), and p-SiNW (d); H-n-^{P}SiNW (e), H-n-SiNW (f), H-p-^{P}SiNW (g), and H-p-SiNW (h). The scale bars for all images are 100 nm.

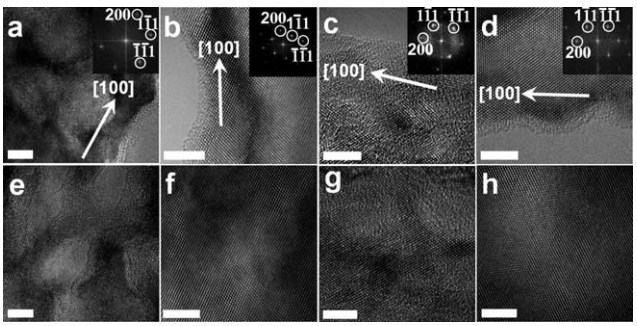

Fig. 4 HRTEM images of edge and interior of the single H-n-^{P}SiNWs (a and e), H-n-SiNWs (b and f), H-p-^{P}SiNWs (c and g), and H-p-SiNWs (d and h). The scale bars for all images are 5 nm.

and 4f) and H-p-SiNWs (Fig. 4d and 4h). The results are consistent with the normal TEM images. The cores in all kinds of SiNWs are single crystalline, although the surfaces are rough and covered with very thin amorphous layers. The insets show the diffraction patterns converted by fast Fourier transform (FFT) from their corresponding HRTEM images with the edge areas. In addition, FFT patterns combined with standard XRD and crystal lattice images indicate that all kinds of SiNWs have the same growth direction of [100], which is also the surface orientation of their mother wafers.

To probe the texture properties of SiNWAs, nitrogen adsorption-desorption isotherms and the corresponding pore-size distributions of the as-synthesized samples of p-^{P}SiNWAs and p-SiNWAs were performed. The isotherm of p-^{P}SiNWAs shown in Fig. 5a is of type IV, a characteristic of mesoporous materials, according to the IUPAC classification. The adsorption isotherm of the p-^{P}SiNWAs exhibits a sharp increase in the $P/P_0 = 0.82$–1.00, corresponding to capillary condensation within mesopores, revealing that the narrow pore-size distribution of the synthesized p-type porous SiNWs. Multipoint BET analysis of adsorption isotherm yields a surface area up to 332 $m^2\ g^{-1}$ and a large total pore volume of 1.08 $cm^3\ g^{-1}$ at the relative P/P_0 of 0.99. Correspondingly, as shown in Fig. 5b, the BJH pore size of the as-synthesized p-^{P}SiNWAs ranging from 2 to 20 nm is centered at 6.3 nm. In contrast, the nonporous sample of p-SiNWAs possesses a BET surface area of only 30 $m^2\ g^{-1}$ and no porosity is observed in the pore size distribution curves (Fig. 5b). The isotherms of the as-synthesized n-^{P}SiNWAs and n-SiNWAs are similar to those of p-^{P}SiNWAs and p-SiNWAs, respectively (not shown in the paper). As shown in Table 1, the surface area and total pore volume of porous n-^{P}SiNWAs is 330 $m^2\ g^{-1}$ and 0.92 $cm^3\ g^{-1}$, respectively, with pore size ranging from 3 to 20 nm and centered at 5.5 nm based on the BJH model. In contrast, the surface area and total volume of nonporous n-SiNWAs is only 26 $m^2\ g^{-1}$ and 0.08 $cm^3\ g^{-1}$, respectively. These results are consistent with the TEM analysis.

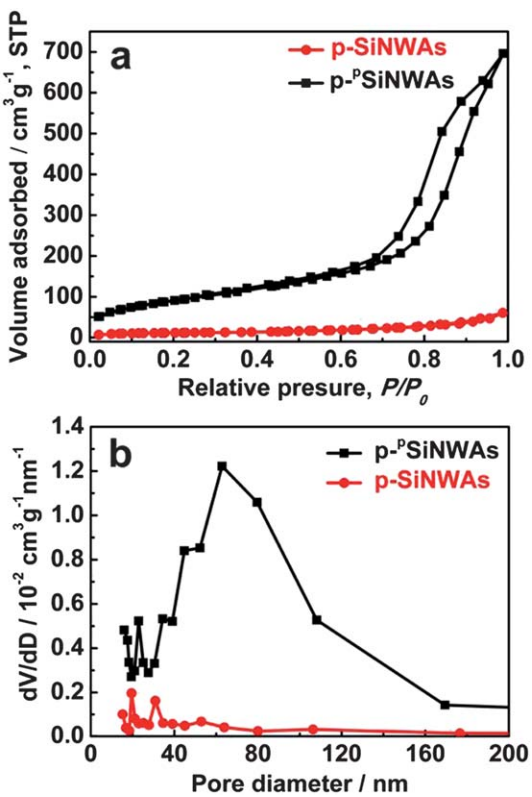

Fig. 5 Nitrogen adsorption measurements of porous and nonporous SiNWAs. (a) typical nitrogen adsorption isotherms of porous p-^{P}SiNWAs and nonporous p-SiNWAs samples; (b) typical BJH pore size distributions for porous p-^{P}SiNWAs and nonporous p-SiNWAs samples.

The formation mechanisms of porous and nonporous SiNWs by the two-step method were proposed by Duan *et al.*:[28,41] 1) AgNPs are firstly deposited on the surface of a Si wafer which act as the cathode and catalyst, and the Si acts as the anode to form an electrochemical cell; 2) during the etching process, AgNPs are partially oxidized to form Ag^+ by H_2O_2 and dissolved. Before diffusing out, the dissolved Ag^+ ions can be quickly reduced back to AgNPs by taking electrons from the interface of Ag and Si, and as a result Ag^+ ions are confined proximately to AgNPs. As the Si dissolves in the etchant, pits are etched by AgNPs and Si below Ag particles is continuously ethched down to form SiNWs; 3) when the concentration of H_2O_2 is high enough, more Ag^+ can be oxidized and part of them diffuse upwards from the roots and renucleate on the sidewalls of the SiNWs. These AgNPs newly renucleated can serve as the new etching sites. It is found that the etching rate of Si wafers with higher dopant concentration is higher, which leads to more effective Ag nuleation. As a result, heavily doped Si wafers with more dopant defects, have high etching rate and produce more AgNPs on the nanowire sidewalls which act as effective etching sites to form the porous structure. On the contrary, on the lightly doped Si wafers, few AgNPs are formed on the SiNWs sidewalls due to low defects concentration. Besides, in the slow Si etching rate, the AgNPs may be readily oxidized back to Ag^+ ions by H_2O_2. In this case, the AgNPs may not be able to serve as effective etching sites or only etch a small portion of the nanowire surface.

Insufficient light harvesting seriouly affects the performance of photocatalysts and photovoltaic devices. In order to suppress the undesired reflections, an additional layer with a thickness of quarter-wavelength is usually employed as the antireflection coating. However, He *et al.* fabricated various nanostructures such as ZnO arrays, SiNWAs and Si nanorod arrays with certain length on the substrate surface directly, which significantly reduced the reflectance.[31,42,43] In this work, absorption spectra of the porous and nonporous SiNWAs are studied. As shown in Fig. 6, the absorption spectra of the four kinds of SiNWAs span across the entire UV and visible light which indicates that the

Table 1 Textural properties of the as-synthesized SiNWAs

Sample	SBET/$m^2\ g^{-1}$ [a]	DBJH/nm [b]	Vpore/$cm^3\ g^{-1}$ [c]
n-^{P}SiNWAs	320	4.4	0.92
n-SiNWAs	26	—	0.08
p-^{P}SiNWAs	332	6.3	1.08
p-SiNWAs	30	—	0.09

[a] Multi-point BET surface area. [b] Pore size as determined from the maximum of the pore-size distribution curve calculated by the BJH model using adsorption branch. [c] Total pore volume at $P/P_0 = 0.989$.

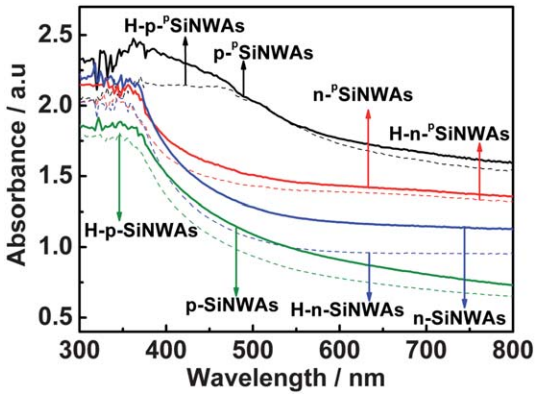

Fig. 6 Absorption spectra of the porous and nonporous SiNWAs.

photocatalytic reactions using SiNWAs as catalysts are effective under the visible light. Obviously, the adsorption intensity of porous SiNWAs is stronger, especially at visible areas, than that of the nonporous ones with the same wafer's area. Presumably, the larger surface area of the porous SiNWAs, the more light can be absorbed. After the HF-treatment, the intensities of all absorption spectra decrease slightly. The reason may be due to the removal of silicon oxide layers on the nanowires which can act as antireflective layer to ensure the light adsorption.[44,45]

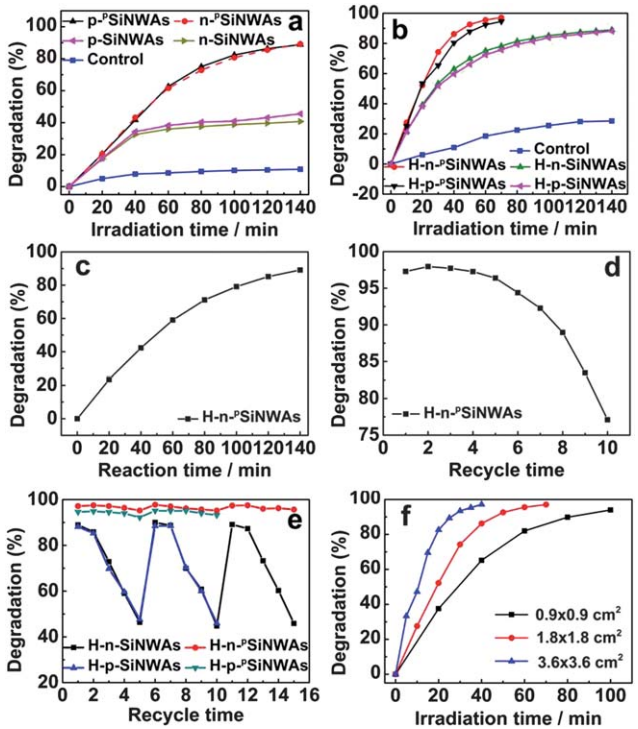

Fig. 7 (a) Comparison of MR photodegradation by porous SiNWAs, nonporous SiNWAs, and self-degradation (control). (b) MR photodegradation of HF-treated porous, nonporous SiNWAs and HF-treated n-type heavily doped Si wafer (control). (c) MR degradation of H-n-PSiNWAs in dark. (d) Recycling experiments of H-n-PSiNWAs in degradation of MR. (e) Comparison of reuse ability of porous and nonporous H-SiNWAs in degradation of MR. (f) MR degradation comparison of H-n-PSiNWAs with different wafer area.

Photocatalytic acitivities of porous and nonporous SiNWAs

With stronger absorption intensity and porous structure, the porous SiNWs and H-SiNWs are expected to be an effective photocatalyst under the visible light. To evaluate the photocatalytic activity of porous and nonporous SiNWs, series of experiments were carried out for the photodegradation of MR and the results are summarized in Fig. 7a. After 140 min of irradiation, the degraded MR are about 89.2%, 88.8%, 45.5% and 40.8% for p-PSiNWAs, n-PSiNWAs, p-SiNWAs and n-SiNWAs, respectively. In contrast, only 10.8% of MR were degraded in the two control experiments without using any catalyst and using n-type heavily doped Si the wafer as catalyst. The results demonstrate that the four kinds of SiNWs are effective photocatalysts with visible light irradiation and that the porous SiNWs have higher efficiency than the nonporous ones. The higher catalytic activity of porous SiNWs is attributed to their larger surface area and more light absorption.

The mechanism using SiNWs as photocatalysts in photodegrading dye compound is commonly known as follows. When a SiNW absorbs a photon of light with energy equal to or larger than its band gap, an electron-hole (e^-/h^+) pair is formed and then separated (eqn (1)), which further react with adsorbed water and dissolved oxygen to produce •OH radicals (eqns, 2–6) which are strong and nonselective oxidizing agents for organic pollutants.[29,46] Finanly, the MR molecules can be oxidized and decomposed by the •OH radicals (eqn (7)).

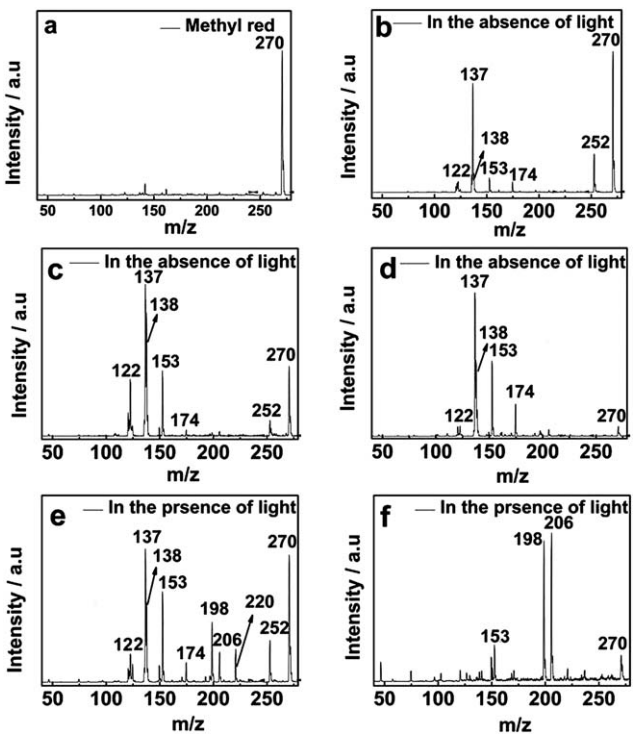

Fig. 8 Mass spectra of original MR solution (a); samples in the absence of light, with H-n-PSiNWAs, and reaction time of 60 (b), 120 (c) and 300 min (d), respectively; samples in the presence of light, with H-n-PSiNWAs and reaction time of 40 and 120 min, respectively. The *m/z* scaning range is from 40 to 280.

Table 2 Proposed chemical structures and ion masses of methyl red and by-products identified in the presence and absence of light with H-n-^{p}SiNWAs

MR/By-product	Chemical structure	Molecular weight	$[M + H]^+/[M + Na]^+$
MR	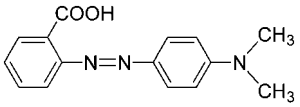	269	270
A	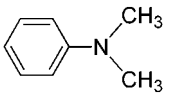	121	122
B	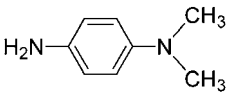	136	137
C	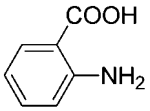	137	138
D	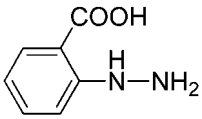	152	153/174
E	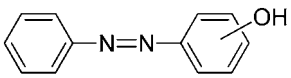	198	199/220
F	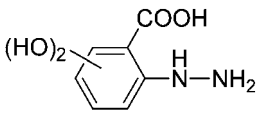	184	206
G	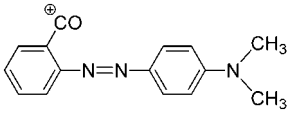	252	252

$$\text{SiNWAs} \xrightarrow{h\nu} h^+ + e^- \quad (1)$$

$$h^+ + H_2O \rightarrow HO\bullet + H^+ \quad (2)$$

$$e^- + O_2 \rightarrow \bullet O_2^- \quad (3)$$

$$\bullet O_2^- + H^+ \rightarrow HOO\bullet \quad (4)$$

$$e^- + HOO\bullet + H^+ \rightarrow H_2O_2 \quad (5)$$

$$H_2O_2 + e^- \rightarrow HO\bullet + OH^- \quad (6)$$

$$HO\bullet + MR \rightarrow \text{intermediates} \rightarrow \text{degradation products} \quad (7)$$

However, the H-SiNWs samples were found to decolor the dye solution as well even in the absence of photo-irradiation. It has been demonstrated that the Si–H bond has highly reductive activity,[47–49] which may reduce the MR molecule directly. To shed light to further explore the catalytic mechanisim here, we performed studies on the degradation process of MR in the presence and absence of light with H-n-^{p}SiNWAs and mass spectrometry was applied to indentify the chemical composition of the degradated sample solution. As shown in Fig. 8a, there is only one main *m*/*z* peak of 270 for the original MR solution. The by-products produced at various reaction times are labled in Table 2 as A to G. In the absence of light, comparing to the spectrum of methyl red, six new *m*/*z* peaks appear in the mass spectrum of the sample solution after being reacted for 60 min (shown in Fig. 8b) and the relative mass intensity of MR is stronger than the new peaks. The peaks with *m*/*z* of 122 and 153 indicate that C–N bonds between the aromatic ring and azo bond are facile to rupture by highly reductive Si–H bonds to yield by-products A and D.[47–50] The peak at 174 corresponds to $[D + Na]^+$. The peaks of 137 and 138 can be attributed to substituted aromatic amines of by-products B and C, which indicate that the degradation proceeded through the cleavage of azo group connected to two aromatic rings. Besides, the peak of 252 (labeled as by-product G) derives from the dehydrated MR molecule (shown in Fig. 8b). With extending reaction time (120 and 300 min, respectively), the mass intensity ratio between the by-products and MR increases continually and the relative mass intensity of MR becomes weaker and weaker, which means MR molecules are keeping reduced (shown in Fig. 8c and 8d). In the presence of light, the mass spectrum shows a substantial difference from the

one in the absense of light. Besides the six peaks mentioned above, three new peaks come forth with value of 198, 206 and 221 in association with •OH radicals produced by SiNWs under irradiation for the first 40 min (shown in Fig. 8e). After 120 min irradiation, the peaks of 122, 137, 138, 153, 174 and 252 are completely suppressed, leaving peaks at 198 and 206 as the most intense ones (shown in Fig. 8f). We have to pointed out that the intensity of the peaks in the mass spectra are in relative values; therefore, we cannot compare them directly with each other. However, by combining the UV–Vis absorption spectra, where the absorption of N=N group at 515 nm falls to almost zero after 120 min irradiation, we can conclude the concentration of the presented azobenzene compound E with *m*/*z* of 198 might be neglectably low and almost all compounds have been decomposed to very small molecules (*m*/*z* < 50).

Above all, the reaction pathway in the presence and in the absence of light is quite different. In the absence of light, the reduction occurs simply by hydrogen transfer. While, in the presence of light, a part of MR molecules may be oxidized directly by •OH radicals.[25,26] Some of the MR molecules can be reduced by hydrogen transfer first and then decomposed by •OH radicals. We also noted that SiNWs can produce •OH radicals more easily by hydrogen terminated treatment, which also plays an important role in decomposing MR.[26]

The photocatlytic mechanisim could be further supported by comparing the photocatalytic activity of H-SiNWs with that of the as-synthesized SiNWs. As shown in Fig. 7b, using HF-treated n-type heavily doped Si wafer as the catalyst, only 28.5% MR was decomposed in the control experiment, which was more inactive than HF-treated SiNWAs. It is clear that HF-treated SiNWAs have better catalytic efficiency than the as-synthesized ones. By using the hydrogen-terminated porous and nonporous SiNWAs, about 95% and 75% MR was degraded in 70 min, respectively. Even though the reaction time was further prolonged to 140 min, the MR was only degraded less than 90% by using the two nonporous H-SiNWAs. The improved catalytic efficiency of H-SiNWAs after HF-treatment is resulted from more Si-H bonds on the surface of the SiNWs.[51–54]

In addition to the high catalytic efficiency, the H-SiNWAs possessed robust stability, and retained high catalytic activity after several recycle times. The photodegradation of MR was monitored for several consecutive cycles in 70 and 140 min each for porous H-SiNWAs and nonporous H-SiNWAs, respectively. After each cycle, the samples were taken out and washed thoroughly with DI water before new test. Fig. 7d presents the variation of dye degradation rate with recycle times using the H-n-^{p}SiNWAs as catalyst, which shows more than 95% degradation rate in the first 5 recycle times and maintains high degradation rate (>75%) up to 10 recycles. In contrast, the degradation activity of nonporous SiNWAs quickly dropped to ~40% in 5 recycles (Fig. 7e). As shown in Fig. 7e, it should be highlighted that the degradation activity of all four kinds of SiNWAs could be regenerated by HF-treatment. It is noted that the degradation activity of H-n-^{p}SiNWAs is highly stable (~95%) within 15 recycle times when regenerated every 5 times, while that of H-n-SiNWAs drops abruptly even after HF treatment. The high stability and activity of porous SiNWAs in degradation are ascribed to more active sites produced by HF-treatment. On the other hand, the degradation rate of MR was obviously enhanced with higher wafer area. As shown in Fig. 7f, ~95% of MR was degraded in 100, 70, and 40 min using H-n-^{p}SiNWAs with wafer areas of 0.9 × 0.9, 1.8 × 1.8, and 3.6 × 3.6 cm^2, respectively.

Conclusions

Porous and nonporous SiNWAs with different doping concentrations were prepared *via* the chemical etching method and the photocatalytic performances were systematically studied. All four kinds of SiNWAs exhibited a good photocatalytic activity. The photocatalytic activity of porous SiNWAs is about two times higher than that of the nonporous SiNWAs at the reaction time of 140 min, due to their large surface area, high pore volume, and good visible light absorption properties. After HF-treatment, the photocatalytic activity of all four kinds of SiNWAs was improved distinctively. The improved photocatalytic activity could be mainly attributed to the hydrogen atoms on the H-SiNW's surface which can produce many more •OH radicals and have high reductive activity. In addition, hydrogen-terminated porous SiNWAs possess high stability and catalytic activity within at least 10 recycle times. The photocatalytic activity of four kinds H-SiNWAs can be recovered by HF-treatment. This new kind of porous SiNWAs will have more applications in future.

Acknowledgements

This work was supported by the Department of Biology and Chemistry in the City University of Hong Kong and was finacially supported by City University of Hong Kong (Project Nos.: 7200203, 7002597).

References

1 D. Chen, Z. Jiang, J. Geng, Q. Wang and D. Yang, *Ind. Eng. Chem. Res.*, 2007, **46**, 2741.
2 S. K. Pardeshi and A. B. Patil, *J. Hazard. Mater.*, 2009, **163**, 403.
3 G. S. Shao, F. Y. Wang, T. Z. Ren, Y. P. Liu and Z. Y. Yuan, *Appl. Catal., B*, 2009, **92**, 61.
4 G. S. Shao, L. Liu, T. Y. Ma, F. Y. Wang, T. Z. Ren and Z. Y. Yuan, *Chem. Eng. J.*, 2010, **160**, 370.
5 R. Asahi, T. Morikawa, T. Ohwaki, K. Aoki and Y. Taga, *Science*, 2001, **293**, 269.
6 H. B. Pan, F. Wang, J. L. Huang and N. S. Chen, *Acta Phys.-Chim. Sin.*, 2008, **24**, 992.
7 D. S. Bhatkhande, V. G. Pangarkar and A. A. C. M. Beenackers, *J. Chem. Technol. Biotechnol.*, 2001, **77**, 102.
8 J. S. Hu, L. L. Ren, Y. G. Guo, H. P. Liang, A. M. Cao, L. J. Wan and C. L. Bai, *Angew. Chem., Int. Ed.*, 2005, **44**, 1269.
9 L. S. Zhong, J. S. Hu, A. M. Cao, Q. Liu, W. G. Song and L. J. Wan, *Chem. Mater.*, 2007, **19**, 1648.
10 M. W. Shao, H. Wang, M. L Zhang, D. D. D. Ma and S. T. Lee, *J. Appl. Phys.*, 2008, **93**, 243110.
11 F. X. Wang, M. W. Shao, L. Cheng, D. Y. Chen, Y. Fu and D. D. D. Ma, *Mater. Res. Bull.*, 2009, **44**, 126.
12 S. H. Xu, D. L. Feng and W. F. Shangguan, *J. Phys. Chem. C*, 2009, **113**, 2463.
13 A. O. Ibhadon, G. M. Greenway, Y. Yue, P. Falaras and D. Tsoukleris, *Appl. Catal., B*, 2008, **84**, 351.
14 L. Liu, H. J. Liu, Y. P. Zhao, Y. Q. Wang, Y. Q. Duan, G. D. Gao, M. Ge and W. Chen, *Environ. Sci. Technol.*, 2008, **42**, 2342.
15 Y. G. Guo, J. S. Hu, H. P. Liang, L. J. Wang and C. L. Bai, *Adv. Funct. Mater.*, 2005, **15**, 196.
16 K. H. Yoo, K. S. Kang, Y. Chen, K. J. Han and J. Kim, *Nanotechnology*, 2008, **19**, 505202.
17 H. J. Zhang, G. H. Chen and D. W. Bahnemann, *J. Mater. Chem.*, 2009, **19**, 5089.

18 Y. Huang, X. F. Duan, Y. Cui, L. J. Lauhon, K. H. Kim and C. M. Lieber, *Science*, 2001, **294**, 1313.
19 J. C. Ho, R. Yerushalmi, Z. A. Jacobson, Z. Y. Fan, R. L. Alley and A. Javey, *Nat. Mater.*, 2008, **7**, 62.
20 Y. He, Z. H. Kang, Q. S. Li, C. H. A. Tsang, C. H. Fan and S. T. Lee, *Angew. Chem., Int. Ed.*, 2009, **48**, 128.
21 K. Q. Peng, X. Wang and S. T. Lee, *Appl. Phys. Lett.*, 2008, **92**, 163103.
22 M. L. Zhang, I. Mahmood, X. Fan, G. Xu and N. B. Wong, *J. Nanosci. Nanotechnol.*, 2010, **10**, 8271.
23 A. M. Morales and C. M. Lieber, *Science*, 1998, **279**, 208.
24 Z. H. Kang, C. H. A. Tsang, N. B. Wong, Z. D. Zhang and S. T. Lee, *J. Am. Chem. Soc.*, 2007, **129**, 12090.
25 Z. H. Kang, Y. Liu, C. H. A. Tsang, D. D. D. Ma, X. Fan, N. B. Wong and S. T. Lee, *Adv. Mater.*, 2009, **21**, 661.
26 M. W. Shao, L. Cheng, X. Zhang, D. D. D. Ma and S. T. Lee, *J. Am. Chem. Soc.*, 2009, **131**, 17738.
27 N. Megouda, Y. Cofininier, S. Szunerits, T. Hadjersi, O. ElKechai and R. Boukherroub, *Chem. Commun.*, 2011, **47**, 991.
28 Y. Q. Qu, L. Liao, Y. J. Li, H. Zhang, Y. Huang and X. F. Duan, *Nano Lett.*, 2009, **9**, 4539.
29 Y. Q. Qu, X. Zhong, Y. J. Li, L. Liao, Y. Huang and X. F. Duan, *J. Mater. Chem.*, 2010, **20**, 3590.
30 A. I. Hochbaum, D. Gargas, Y. J. Hwang and P. D. Yang, *Nano Lett.*, 2009, **9**, 3550.
31 Y. A. Dai, H. C. Chang, K. Y. Lai, C. A. Lin, R. J. Chung, G. R. Lin and J. H. He, *J. Mater. Chem.*, 2010, **20**, 10924.
32 K. Q. Peng, Y. Wu, H. Fang, X. Y. Zhang, Y. Xu and J. Zhu, *Angew. Chem., Int. Ed.*, 2005, **44**, 2737.
33 H. P. Wang, K. Y. Lai, Y. R. Lin, C. A. Lin and J. H. He, *Langmuir*, 2010, **26**, 12855.
34 H. C. Chang, K. Y. Lai, Y. A. Dai, H. H. Wang, C. A. Lin, and J. H. He, *Energy Environ. Sci.* DOI: 10.1039/C0EE00595A.
35 M. L. Zhang, K. Q. Peng, X. Fan, J. S. Jie, R. Q. Zhang, S. T. Lee and N. B. Wong, *J. Phys. Chem. C*, 2008, **112**, 4444.
36 K. Y. Lai, Y. R. Lin, H. P. Wang and J. H. He, *CrystEngComm*, 2011, **13**, 1014.
37 A. M. Morales and C. M. Lieber, *Science*, 1998, **279**, 208.
38 Y. Cui, X. F. Duan, J. T. Hu and C. M. Lieber, *J. Phys. Chem. B*, 2000, **104**, 5213.
39 Y. F. Zhang, Y. H. Tang, C. Lam, N. Wang, C. S. Lee, I. Bello and S. T. Lee, *J. Cryst. Growth*, 2000, **212**, 115.
40 J. B. Hannon, S. Kodambaka, F. M. Ross and R. M. Tromp, *Nature*, 2006, **440**, 69.
41 X. Zhong, Y. Q Qu, Y. C. Lin, L. Liao and X. F Duan, *ACS Appl. Mater. Interfaces*, 2011, **3**, 261.
42 Y. C. Chao, C. Y. Chen, C. A. Lin, Y. A. Dai and J. H. He, *J. Mater. Chem.*, 2010, **20**, 8134.
43 Y. R. Lin, K. Y. Lai, H. P. Wang and J. H. He, *Nanoscale*, 2010, **2**, 2765.
44 N. Terada, T. Haga, N. Miyata and K. Moriki, *Phys. Rev. B: Condens. Matter*, 1992, **46**, 2312.
45 E. C. Cho, J. Xia, A. G. Aberle and M. A. Green, *Sol. Energy Mater. Sol. Cells*, 2002, **74**, 31.
46 I. K. Konstantinou and T. A. Albanis, *Appl. Catal., B*, 2004, **49**, 1.
47 X. H. Sun, H. Y. Peng, Y. H. Tang, W. S. Shi, N. B. Wong, C. S. Lee and S. T. Lee, *J. Appl. Phys.*, 2001, **89**, 6396.
48 C. H. A. Tsang, Y. Liu, Z. H. Kang, D. D. D. Ma, N. B. Wong and S. T. Lee, *Chem. Commun.*, 2009, 5829.
49 X. H. Sun, C. P. Li, N. B. Wong, C. S. Lee, S. T. Lee and B. K. Teo, *J. Am. Chem. Soc.*, 2002, **124**, 14856.
50 F. Wu, N. S. Deng and H. L. Hua, *Chemosphere*, 2000, **41**, 1233.
51 X. H. Sun, S. D. Wang, N. B. Wong, D. D. D. Ma and S. T. Lee, *Inorg. Chem.*, 2003, **42**, 2398.
52 B. K. Teo, W. W. Chen, X. H. Sun, S. D. Wang and S. T. Lee, *J. Phys. Chem. B*, 2005, **109**, 21716.
53 W. W. Chen, X. H. Sun, S. D. Wang, S. T. Lee and B. K. Teo, *J. Phys. Chem. B*, 2005, **109**, 10871.
54 C. S. Guo, L. B. Luo, G. D. Yuan, X. B. Yang, R. Q. Zhang, W. J. Zhang and S. T. Lee, *Angew. Chem., Int. Ed.*, 2009, **48**, 9896.